Hindawi
International Journal of Antennas and Propagation
Volume 2023, Article ID 8622428, 12 pages
https://doi.org/10.1155/2023/8622428

Research Article

A Low-Complexity Direction-of-Arrival Estimation Algorithm for Noncircular Signals via Subspace Rotation Technique

Wei Wang,[1] **Ming Zhang**,[2] **Bobin Yao**,[3] **Tongxing Zheng**,[4] **and Xiaojiao Fan**[1]

[1]*School of Computer Science, XiJing University, Xi'an 710123, China*
[2]*Xi'an Microelectronics Technology Institute, Xi'an 710000, China*
[3]*School of Electronic and Control Engineering, Chang'an University, Xi'an 710064, China*
[4]*School of Electronic and Information Engineering, Xi'an Jiaotong University, Xi'an 710049, China*

Correspondence should be addressed to Wei Wang; amywang198611@163.com

Received 7 November 2022; Revised 7 March 2023; Accepted 8 March 2023; Published 21 March 2023

Academic Editor: Atsushi Mase

In this paper, we investigate the problem of the heavy computational burden of the direction-of-arrival (DoA) estimation for the noncircular (NC) signals. A novel low-complexity direction-of-arrival estimation algorithm for NC signals via subspace rotation technique (SRT) is proposed. The proposed algorithm divides the noise subspace matrix along its row direction into two submatrices, and the SRT is performed to get a new reduced-dimension noise subspace. Then, utilizing the separation of variables and the orthogonality between the reduced-dimension noise subspace and the space spanned by the columns of the extended manifold matrix, a new one-dimensional spectral search function is derived to estimate DoAs. As the size of the block matrices of the noise subspace matrix has a great impact on the computational complexity of the spectral search, the optimal number of rows of the block matrices is determined. The proposed algorithm not only avoids the two-dimensional spectral search but also efficiently removes the redundancy computations in the one-dimensional spectral search. Theoretical analysis and simulation results show that the proposed algorithm can significantly improve the computational efficiency on the premise of ensuring the accuracy of DoA estimation for the NC signals, especially in scenarios where large numbers of sensors are applied.

1. Introduction

Direction-of-arrival (DoA) estimation has been widely used in various communication applications such as radar, sonar, target location, and wireless communication, which is an extremely important topic in the field of array signal processing [1–9]. High resolution methods for DoA estimation include multiple signal classification (MUSIC) [10], root-multiple signal classification (Root-MUSIC) [11], estimating signal parameters via rotational invariance techniques (ESPRIT) [12], and so forth. However, these traditional algorithms based on the premise of the narrow-band or wide-band sources have not exploited the properties of the incoming sources [13–16]. As the noncircular (NC) signals such as binary phase shift keying (BPSK) signals, amplitude modulation (AM) signals, and multiple amplitude shift keying (MASK) signals have been more and more widely utilized in practical communication, the NC property of incoming sources has been considered in DOA estimation [17–20]. The knowledge of the elliptic covariance matrix, which is not equal to zero, can be used to improve the estimation performance by increasing the dimension of the received signal matrix and extending the array aperture. A two-dimensional noncircular MUSIC (2D-NC-MUSIC) algorithm exploiting the NC property of the incoming sources was proposed in [21], which needs a two-dimensional spectral search, bringing huge computational complexity. In order to decrease the computational complexity of the 2D-NC-MUSIC algorithm, the noncircular MUSIC (NC-MUSIC) algorithm was also presented in [21] to convert the two-dimensional spectral search into the one-dimensional spectral search. A polynomial rooting NC-MUSIC algorithm proposed in [22] can replace the two-dimensional spectral search with the polynomial rooting so

as to reduce the computational complexity of the 2D-NC-MUSIC algorithm to some extent. In [23–25], convex optimization was utilized to avoid the two-dimensional spectral search and greatly improves the computational effectively. However, the required one-dimensional spectral search still has the high computational cost. A SRTRD-NC-MUSIC algorithm was presented in [26], which enhances the computational efficiency by means of the conversion of the two-dimensional peak searching into the one-dimensional peak searching and the removal of some redundancy computations of the one-dimensional peak searching, but still remains redundancy computations in peak searching. Based on the sparsity of target azimuth information in the spatial domain, the methods proposed in [27, 28] use the spatial dictionary and the sparse signal reconstruction to finish the DoA estimation, which can reduce the computational complexity only on the premise of precisely compensating for the NC phase caused by transmission delay.

In order to reduce the computational complexity of the 2D-NC-MUSIC algorithm, we improve the SRTRD-NC-MUSIC algorithm and propose a novel low-complexity DoA estimation algorithm called the SRTRD-p-NC-MUSIC algorithm, which can further avoid redundancy computations in spectral search. In this paper, we divide the noise subspace matrix along its row direction into two submatrices and the subspace rotation technique (SRT) [29] is used to construct a new reduced-dimension noise subspace. As the new reduced-dimension noise subspace is also orthogonal to the space spanned by the columns of the extended manifold matrix, a new one-dimensional spectral search function is finally derived to estimate DOAs by means of the separation of variables. Considering that the size of the block matrices of the noise subspace matrix has a great impact on the dimensions of the new reduced-dimension noise subspace and the computational complexity of the spectral search, we have a discussion about the numbers of rows of the block matrices, and the optimal number of rows of the block matrices is derived. The SRTRD-p-NC-MUSIC algorithm can reduce the computational complexity to less than 3% as compared to the 2D-NC-MUSIC algorithm on the premise of ensuring the accuracy of DOA estimation. Especially, the efficiency advantage of the new algorithm is more obvious for the case that large numbers of sensors are required.

1.1. Notation. Throughout the paper, we utilize upper-case bold letters to denote matrices (e.g., A), lower-case bold letters for vectors (e.g., a) and upper-case double-line characters for sets (e.g., $\mathbb{C}$). $(\cdot)^*$, $(\cdot)^T$, $(\cdot)^H$, and $(\cdot)^\dagger$ represent complex conjugate, transpose, conjugate transpose, and pseudoinverse, respectively. $E\{\cdot\}$ is used to represent the statistical expectation. $\|.\|$ and det $(\cdot)$, respectively, indicate the norm of a vector and the determinant of a matrix. diag $\{.\}$ stands for a diagonal matrix composed of the embraced elements. Span $(\cdot)$ is the space spanned by the columns of a matrix, dim $(\cdot)$ is the dimension of a linear space and rank $(\cdot)$ is the rank of a matrix. I_M represents a $M \times M$ identity matrix and $0_{M\times N}$ denotes a $M \times N$ matrix with all zero elements.

2. Data Model and 2D-NC-MUSIC Algorithm

2.1. Data Model. The noncircular signals have been extensively used in various modern communication systems. As the noncircular signals have the property that the pseudo-covariance is nonzero, the effective array aperture can be extended by means of increasing the number of virtual sensors [17–20]. Considering the impact of the actual transmission channel, the received signals can be represented as

$$S(t) = S_R(t)e^{j\varphi}, \tag{1}$$

where $S_R(t)$ is the real signal, and the phase φ is the sum of the initial phase of the signal and the additional phase of the transmission channel. Consider an M-element uniform linear array (ULA) with the interelement spacing d and select the leftmost sensor of the ULA as the reference one. K independent narrow-band far-field noncircular signals $S_k(t)$ $(k = 1, 2, \ldots, K)$ are impinging on the ULA from the different directions θ_k $(k = 1, 2, \ldots, K)$, as shown in Figure 1. The received signals of the ULA can be expressed as

$$\mathbf{X}(t) = \mathbf{A}\mathbf{S}(t) + \mathbf{N}(t) = \mathbf{A}\Psi\mathbf{S}_R(t) + \mathbf{N}(t), \tag{2}$$

where $\mathbf{S}(t) = [S_1(t), S_2(t), \cdots, S_K(t)]^T \in \mathbb{C}^{K\times 1}$ is the noncircular incident signal vector, $\mathbf{A} = [\mathbf{a}(\theta_1), \mathbf{a}(\theta_2), \cdots, \mathbf{a}(\theta_K)] \in \mathbb{C}^{M\times K}$ is the manifold matrix with the steering vector $\mathbf{a}(\theta_k) = [1, e^{j2\pi d \sin\theta_k/\lambda}, \cdots, e^{j2\pi(M-1)d\sin\theta_k/\lambda}]^T$ $(k = 1, 2, \ldots, K)$ and λ is the wavelength of the carrier wave. $\mathbf{N}(t) = [n_1(t), n_2(t), \cdots, n_M(t)]^T \in \mathbb{C}^{M\times 1}$ represents the white Gaussian noise vector with zero mean and variance σ^2. $\mathbf{S}_R(t) = [S_{R,1}(t), S_{R,2}(t), \cdots, S_{R,K}(t)]^{\mathrm{T}} \in \mathbb{R}^{K\times 1}$ and $\Psi = \mathrm{diag}\{e^{j\varphi_1}, e^{j\varphi_2}, \cdots, e^{j\varphi_K}\}$ with φ_k $(k = 1, 2, \cdots, K)$ being the noncircular phase of the kth incident signal.

Considering that a noncircular signal has the characteristics of $E\{\boldsymbol{S}(t)\boldsymbol{S}^T(t)\} \neq 0$ and $E\{\mathbf{S}^*(t)\boldsymbol{S}^H(t)\} \neq 0$, we concatenate the array output and its conjugation to increase the number of available sensors [13–20]. So a new extended vector is obtained, as shown in the following:

$$\begin{aligned}\mathbf{Y}(t) &= \begin{bmatrix}\mathbf{X}(t)\\ \mathrm{X}^*(t)\end{bmatrix}\\ &= \begin{bmatrix}\mathbf{A}\Psi\\ \mathbf{A}^*\Psi^*\end{bmatrix}\mathbf{S}_R(t) + \begin{bmatrix}\mathbf{N}(t)\\ \mathbf{N}^*(t)\end{bmatrix}\\ &= \mathbf{B}\mathbf{S}_R(t) + \mathbf{N}_0(t),\end{aligned} \tag{3}$$

where $\mathbf{B} = \begin{bmatrix}(\mathbf{A}\Psi)^T & (\mathbf{A}\Psi)^H\end{bmatrix}^T = [\mathbf{b}(\theta_1,\varphi_1), \mathbf{b}(\theta_2,\varphi_2), \cdots, \mathbf{b}(\theta_K,\varphi_K)]$ and $\mathbf{N}_0(t) = \begin{bmatrix}\mathbf{N}^T(t) & \mathbf{N}^H(t)\end{bmatrix}^T$.

2.2. 2D-NC-MUSIC Algorithm. The extended covariance matrix R_Y is expressed as

$$\mathbf{R}_Y = E\{Y(t)Y^H(t)\}. \tag{4}$$

According to the eigenvalue decomposition (EVD) of the matrix R_Y, the label (4) can be further rewritten as

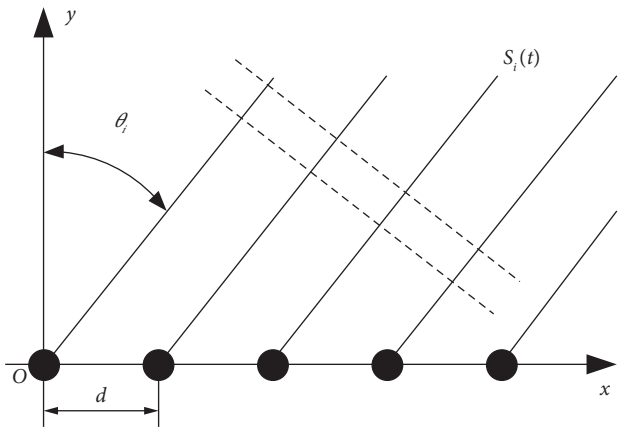

Figure 1: Array signal model.

$$\mathbf{R}_Y = \sum_{i=1}^{K} \lambda_i \mathbf{v}_i \mathbf{v}_i^H + \sum_{i=K+1}^{2M} \lambda_i \mathbf{v}_i \mathbf{v}_i^H = \mathbf{V}_S \mathbf{\Lambda}_S \mathbf{V}_S^H + \mathbf{V}_N \mathbf{\Lambda}_N \mathbf{V}_N^H, \quad (5)$$

where $\lambda_1 \geq \lambda_2 \geq \cdots \geq \lambda_K > \lambda_{K+1} = \lambda_{K+2} = \cdots = \lambda_{2M}$, $\mathbf{\Lambda}_S = \mathrm{diag}\{\lambda_1, \lambda_2, \cdots, \lambda_K\}$, $\mathbf{\Lambda}_S = \mathrm{diag}\{\lambda_{K+1}, \lambda_{K+2}, \cdots, \lambda_{2M}\}$, and $\mathbf{V}_i$ ($i = 1, 2, \ldots, 2M$) is the eigenvector corresponding to the eigenvalue λ_i ($i = 1, 2, \ldots, 2M$). $\mathbf{V}_S = \{\mathbf{v}_1, \mathbf{v}_2, \cdots, \mathbf{v}_K\}$ and $\mathbf{V}_N = \{\mathbf{v}_{K+1}, \mathbf{v}_{K+2}, \cdots, \mathbf{v}_{2M}\}$ are the signal subspace and the noise subspace, respectively. In practice, we usually use the L snapshots of the received signal $X(t)$ to estimate the extended covariance matrix R_Y as follows:

$$\widehat{\mathbf{R}}_Y = \frac{1}{L} \sum_{t=1}^{L} Y(t) Y^H(t). \quad (6)$$

Based on the orthogonality property between the signal subspace and the noise subspace, the two-dimensional NC-MUSIC function can be constructed to estimate the DOAs of the noncircular signals as follows [21]:

$$P_{2D-\mathrm{NC-MUSIC}}(\theta, \varphi) = \frac{1}{\mathbf{b}^{\mathrm{H}}(\theta, \varphi) \widehat{\mathbf{V}}_N \widehat{\mathbf{V}}_N^H \mathbf{b}(\theta, \varphi)}, \quad (7)$$

where

$$\mathbf{b}(\theta, \varphi) = \left[e^{j\varphi}, e^{(j(\varphi + 2\pi d \sin\theta)/\lambda)}, \cdots, e^{(j(\varphi + 2\pi(M-1)d \sin\theta)/\lambda)}, e^{-j\varphi}, e^{-(j(\varphi + 2\pi d \sin\theta)/\lambda)}, \cdots, e^{-(j(\varphi + 2\pi(M-1)d \sin\theta)/\lambda)} \right]^T. \quad (8)$$

The K maxima referring to source DoAs can be obtained by the two-dimensional spectral search. It is observed that although the 2D-NC-MUSIC algorithm can extend the effective array aperture and greatly improve the resolution of the DoA estimation, the expensive computation cost of two-dimension spectral search limits the practical application of the 2D-NC-MUSIC algorithm in the high-real-time processing scenarios [30–32].

3. SRTRD-p-NC-MUSIC Algorithm

In this section, we propose a new algorithm to reduce the computational complexity of the 2D-NC-MUSIC algorithm. We first use the block matrix method and SRT to construct a reduced-dimensional noise space. Then, based on the orthogonality between the reduced-dimensional noise space and the space spanned by the columns of the extended manifold matrix, the separation of variables is utilized to convert the two-dimensional spectral search into the one-dimensional spectral search. Finally, because the number of rows in the block matrices has a great impact on the computational complexity of the proposed algorithm, we discuss about the selection of the number of rows in the block matrices and give the optimum value.

3.1. SRT and Reconstruction of the Noise Subspace. The noise subspace $V_N \in \mathbb{C}^{2M \times (2M-K)}$ can be divided along its row direction into two block matrices, as shown in the following:

$$\mathbf{V}_N = \begin{bmatrix} \mathbf{V}_{N,1} \} M - p \\ 2M-K \\ \mathbf{V}_{N,2} \} M + p \\ 2M-K \end{bmatrix}, \quad (9)$$

where $\mathbf{V}_{N,1} \in \mathbb{C}^{(M-p) \times (2M-K)}$ and $\mathbf{V}_{N,2} \in \mathbb{C}^{(M+p) \times (2M-K)}$. Obviously, $\mathrm{rank}(\mathbf{V}_N) = \dim(\mathrm{span}(\mathbf{V}_N)) = 2M - K$, and if $1 \leq p \leq M - K$, the matrix $\mathbf{V}_{N,2}$ is row full rank. According to the matrix theory [33], we know that the matrix $\mathbf{V}_{N,2}$ has a right inverse matrix $\mathbf{V}_{N,2}^{\dagger}$ satisfying $\mathbf{V}_{N,2}^{\dagger} \mathbf{V}_{N,2}^{\dagger} = \mathrm{I}_{M+p}$. In order to construct the new noise space span ($\mathbf{V}_{\mathrm{new}}$), we use the matrix $\mathbf{V}_{N,2}^{\dagger}$ to weight the column vectors of the noise space $\mathbf{V}_N$ with the following form:

$$\mathbf{V}_{\mathrm{new}} = \mathbf{V}_N \mathbf{V}_{N,2}^{\dagger}. \quad (10)$$

The abovementioned label (10) means we rotate the space span ($\mathbf{V}_N$) by an angle in the $2M$-dimensional space. Consider $\mathrm{rank}(\mathbf{V}_{\mathrm{new}}) \leq \min[\mathrm{rank}(\mathbf{V}_N), \mathrm{rank}(\mathbf{V}_{N,2}^{\dagger})]$, then the new constructed space span ($\mathbf{V}_{\mathrm{new}}$) is a subset of the space span (V_N):

$$\mathrm{span}(\mathbf{V}_{\mathrm{new}}) \subseteq \mathrm{span}(\mathbf{V}_N). \quad (11)$$

As we know, $\mathrm{span}(\mathbf{V}_N) \perp \mathrm{span}(\mathbf{V}_S)$ and $\mathrm{span}(\mathbf{V}_S) = \mathrm{span}(\mathbf{B})$, so the space span (B) is orthogonal to the reconstructed space span ($\mathbf{V}_{\mathrm{new}}$):

$$\mathbf{V}_{\mathrm{new}}^H \mathbf{b}(\theta_i, \varphi_i) = \mathbf{0}_{(M+p) \times 1}, \quad (12)$$

where $i = 1,2, \ldots, K$.

3.2. Construction of the Reduced-Dimension Spectrum Function. Based on the orthogonality property between the reconstructed noise subspace $\mathbf{V}_{\text{new}}$ and the column space spanned by the matrix B, the two-dimensional spectrum function is defined according to label (13) [27]:

$$\begin{aligned} P_{2D}(\theta,\varphi) &= \frac{1}{f(\theta,\varphi)} \\ &= \frac{1}{\mathbf{b}^H(\theta,\varphi)\mathbf{V}_{\text{new}}\mathbf{V}_{\text{new}}^H\mathbf{b}(\theta,\varphi)}. \end{aligned} \tag{13}$$

The estimation of two-dimensional DOAs of noncircular signals can be acquired by searching the minimum of $f(\theta,\varphi)$. Based on the separation of variables, $b(\theta,\varphi)$ is represented as

$$\begin{aligned} \mathbf{b}(\theta,\varphi) &= \begin{bmatrix} \mathbf{a}(\theta)e^{j\varphi} \\ \mathbf{a}^*(\theta)e^{-j\varphi} \end{bmatrix} \\ &= \widetilde{\mathbf{A}}(\theta)\mathbf{E}(\varphi), \end{aligned} \tag{14}$$

where

$$\begin{aligned} \widetilde{\mathbf{A}}(\theta) &= \begin{bmatrix} \mathbf{a}(\theta) & 0_{M\times 1} \\ 0_{M\times 1} & \mathbf{a}^*(\theta) \end{bmatrix}, \\ \mathrm{E}(\varphi) &= \begin{bmatrix} e^{j\varphi} & e^{-j\varphi} \end{bmatrix}^T. \end{aligned} \tag{15}$$

The label (13) can be further rewritten as

$$\begin{aligned} P_{2D}(\theta,\varphi) &= \frac{1}{f(\theta,\varphi)} \\ &= \frac{1}{\mathbf{E}^H(\varphi)\left(\widetilde{\mathbf{A}}^H(\theta)\mathbf{V}_{\text{new}}\mathbf{V}_{\text{new}}^H\widetilde{\mathbf{A}}(\theta)\right)\mathbf{E}(\varphi)}. \end{aligned} \tag{16}$$

Since $\widetilde{\mathbf{A}}^H(\theta)\mathbf{V}_{\text{new}}\mathbf{V}_{\text{new}}^H\widetilde{\mathbf{A}}(\theta)$ is a Hermitian matrix and $f(\theta,\varphi)$ is a nonnegative-definite quadratic form, the minimum of $f(\theta,\varphi)$ can be determined by the minimum eigenvalue of the matrix $\widetilde{\mathbf{A}}^H(\theta)\mathbf{V}_{\text{new}}\mathbf{V}_{\text{new}}^H\widetilde{\mathbf{A}}(\theta)$. When θ is one of the real DOAs of the received signals, the minimum eigenvalue of the matrix $\widetilde{\mathbf{A}}^H(\theta)\mathbf{V}_{\text{new}}\mathbf{V}_{\text{new}}^H\widetilde{\mathbf{A}}(\theta)$ is zero. Then the minimum of the determinant of the matrix $\widetilde{\mathbf{A}}^H(\theta)\mathbf{V}_{\text{new}}\mathbf{V}_{\text{new}}^H\widetilde{\mathbf{A}}(\theta)$ is also zero [31]:

$$\det\left(\widetilde{\mathbf{A}}^H(\theta_i)\mathbf{V}_{\text{new}}\mathbf{V}_{\text{new}}^H\widetilde{\mathbf{A}}(\theta_i)\right) = 0. \tag{17}$$

We construct a new reduced-dimension spectrum function as follows:

$$P_{\text{SRTRD-}p\text{-NC-MUSIC}}(\theta) = \frac{1}{\det\left(\widetilde{\mathbf{A}}^H(\theta)\mathbf{V}_{\text{new}}\mathbf{V}_{\text{new}}^H\widetilde{\mathbf{A}}(\theta)\right)}. \tag{18}$$

By only one-dimensional peak searching, the DOAs of the noncircular signals can be obtained by searching K minimum values of (18).

Compared with the 2D-NC-MUSIC algorithm, the proposed algorithm can not only reduce the dimension of the noise subspace, but also need only one-dimensional peak searching to obtain the estimation of the DOAs of the received signals. The following analysis will show that the proposed SRTRD-p-NC-MUSIC algorithm can significantly reduce the computational complexity of the 2D-NC-MUSIC algorithm and dramatically improve the computational efficiency on the premise of ensuring the accuracy of DoA estimation.

3.3. Simplification of the SRTRD-p-NC-MUSIC Algorithm. Substituting label (9) into label (10), label (10) can be further represented as

$$\begin{aligned} \mathbf{V}_{\text{new}} &= \mathbf{V}_N\mathbf{V}_{N,2}^\dagger \\ &= \begin{bmatrix} \mathbf{V}_{N,1} \\ \mathbf{V}_{N,2} \end{bmatrix}\mathbf{V}_{N,2}^\dagger \\ &= \begin{bmatrix} \mathbf{V}_{N,1}\mathbf{V}_{N,2}^\dagger \\ \mathrm{I}_{M+p} \end{bmatrix} \\ &= \begin{bmatrix} \mathbf{V}_{rot}\}\, M-p \\ {\scriptstyle M+p} \\ \mathrm{I}_{M+p} \end{bmatrix}, \end{aligned} \tag{19}$$

with $\mathbf{V}_{\text{new}} \in \mathbb{C}^{(M-P)\times(M+P)}$. Then, we can divide the matrix $\widetilde{\mathbf{A}}^H(\theta) \in \mathbb{C}^{2\times 2M}$ into block matrices as follows:

$$\tilde{A}^H(\theta) = \begin{bmatrix} \tilde{a}^H(\theta) & e_0^H(\theta) & 0_{1\times M} \\ \underbrace{0_{1\times(M-p)}}_{M\text{-}p} & \underbrace{0_{1\times p} \quad a^T(\theta)}_{M+p} \end{bmatrix} = \left[\begin{array}{c|cc} \tilde{a}^H(\theta) & e_1(\theta) \\ 0_{1\times(M-p)} & e_2(\theta) \end{array}\right], \tag{20}$$

where

$$\begin{aligned} &\tilde{\mathbf{a}}(\theta) = \left[1, e^{j2\pi d\sin\theta/\lambda}, \cdots, e^{j2\pi(M-p-1)d\sin\theta/\lambda}\right]^T \in \mathbb{C}^{(M-p)\times 1}, \\ &\mathbf{e}_0(\theta) = \left[e^{j2\pi(M-p)d\sin\theta/\lambda}, \cdots, e^{j2\pi(M-1)d\sin\theta/\lambda}\right]^T \in \mathbb{C}^{p\times 1}, \\ &\mathbf{e}_1(\theta) = \begin{bmatrix} \mathbf{e}_0^H(\theta) & \mathbf{0}_{1\times M} \end{bmatrix} \in \mathbb{C}^{1\times(M+p)}, \\ &\mathbf{e}_2(\theta) = \begin{bmatrix} \mathbf{0}_{1\times p} & \mathbf{a}^T(\theta) \end{bmatrix} \in \mathbb{C}^{1\times(M+p)}. \end{aligned} \tag{21}$$

Based on label (19) and label (20), we can obtain

$$\begin{aligned} \widetilde{\mathbf{A}}^H(\theta)\mathbf{V}_{\text{new}} &= \begin{bmatrix} \tilde{\mathbf{a}}^H(\theta) & \mathrm{e}_1(\theta) \\ 0_{1\times(M-p)} & \mathrm{e}_2(\theta) \end{bmatrix}\begin{bmatrix} \mathbf{V}_{\text{rot}} \\ \mathrm{I}_{M+p} \end{bmatrix} \\ &= \begin{bmatrix} \tilde{\mathbf{a}}^H(\theta)\mathbf{V}_{\text{rot}} + \mathrm{e}_1(\theta) \\ \mathrm{e}_2(\theta) \end{bmatrix}. \end{aligned} \tag{22}$$

Furthermore, we substitute label (22) into label (18) to get

$$\begin{aligned}\widetilde{\mathbf{A}}^H\mathbf{V}_{\text{new}}\mathbf{V}_{\text{new}}^H\widetilde{\mathbf{A}} &= \begin{bmatrix}\widetilde{\mathbf{a}}^H\mathbf{V}_{\text{rot}} + \mathrm{e}_1\\ \mathrm{e}_2\end{bmatrix}\begin{bmatrix}\mathbf{V}_{\text{rot}}^H\widetilde{\mathbf{a}} + \mathrm{e}_1^H & \mathrm{e}_2^H\end{bmatrix}\\ &= \begin{bmatrix}\left\|\widetilde{\mathbf{a}}^H\mathbf{V}_{\text{rot}}\right\|^2 + 2\mathbf{R}\mathrm{e}\left\{\widetilde{\mathbf{a}}^H\mathbf{V}_{rot}\mathrm{e}_1^H\right\} + \left\|\mathrm{e}_1\right\|^2 & \widetilde{\mathbf{a}}^H\mathbf{V}_{rot}\mathrm{e}_2^H + \mathrm{e}_1\mathrm{e}_2^H\\ \mathrm{e}_2\mathbf{V}_{\text{rot}}^H\widetilde{\mathbf{a}} + \mathrm{e}_2\mathrm{e}_1^H & \left\|\mathrm{e}_2\right\|^2\end{bmatrix}\\ &= \begin{bmatrix}\left\|\widetilde{\mathbf{a}}^H\mathbf{V}_{\text{rot}}\right\|^2 + 2\mathbf{R}\mathrm{e}\left\{\widetilde{\mathbf{a}}^H\mathbf{V}_{\text{rot}}\mathrm{e}_1^H\right\} + p & \widetilde{\mathbf{a}}^H\mathbf{V}_{rot}\mathrm{e}_2^H\\ \mathrm{e}_2\mathbf{V}_{\text{rot}}^H\widetilde{\mathbf{a}} & M\end{bmatrix},\end{aligned} \tag{23}$$

where the tag θ representing the angle is omitted for notational convenience. Then, the proposed SRTRD-NC-MUSIC algorithm can be further simplified, as shown in the following:

$$P_{\mathbf{SRTRD}-p-\mathbf{NC}-\mathbf{MUSIC}}(\theta) = \frac{1}{M\left(\|\boldsymbol{\eta}(\theta)\|^2 + 2\mathbf{R}\mathrm{e}\left\{\boldsymbol{\eta}(\theta)\mathbf{e}_1^H(\theta)\right\} + p\right) - \left\|\boldsymbol{\eta}(\theta)\mathbf{e}_2^H(\theta)\right\|^2}, \tag{24}$$

where $\eta(\theta) = \widetilde{\mathbf{a}}^H(\theta)\mathbf{V}_{\text{rot}}$. From label (24), we can see that the computational complexity of the proposed SRTRD-NC-MUSIC algorithm is greatly affected by the selection of p because of the relation between the value of p and the dimensions of $\eta(\theta)$, $\widetilde{\mathbf{a}}(\theta)$, $\mathbf{V}_{\text{rot}}$, and $\mathbf{e}_1(\theta)$. The following analysis shows that when the value of p is optimal, the proposed SRTRD-NC-MUSIC algorithm can dramatically improve the computational efficiency as compared to the 2D-NC-MUSIC algorithm.

3.4. Optimal Selection of p. In this section, we further discuss about the selection of the value of p to dramatically improve the computational efficiency. Note that the complexities are given in terms of complex-valued flops [26–29]. For the 2D-NC-MUSIC and the SRTRD-p-NC-MUSIC, the EVD of the covariance matrix R_Y can use the fast subspace decomposition (FSD) technique [34], and $O(4M^2K)$ flops are required to use the FSD technique of the covariance matrix R_Y. Compared with the 2D-NC-MUSIC, we need to additionally construct the new noise subspace $\mathbf{V}_{\text{new}}$ and calculate the matrix $\mathbf{V}_{N,2}^{\dagger}$ for the SRTRD-p-NC-MUSIC. As we know, the dimensions of the matrix $\mathbf{V}_{\text{new}}$ and the matrix $\mathbf{V}_{N,2}^{\dagger}$ are $2M \times (2M-K)$ and $(M+p) \times (2M-K)$, respectively. Then, the construction of the matrix $\mathbf{V}_{\text{new}}$ needs O $[(M-p)(M+p)(2M-K)]$ + O $[2M(2M-K)]$ flops [29].

For the 2D-NC-MUSIC and the SRTRD-p-NC-MUSIC, the spectral search step is needed to estimate the DOAs of the received signals. Assuming there are J points within the search range [−90° and 90°] of the incident angle θ and the search range $[0, 2\pi]$ of the noncircular phase φ, respectively, the 2D-NC-MUSIC requires $O[J^2(2M+1)(2M-K)]$ flops to finish the spectral search. For the SRTRD-p-NC-MUSIC, it has to compute $\|\eta\|^2$, $\eta(\theta)\mathrm{e}_1^H(\theta)$, and $\|\eta(\theta)\mathrm{e}_2^H(\theta)\|^2$ for each search point. Then, the cost of computing $\|\eta\|^2$, $\eta(\theta)\mathrm{e}_1^H(\theta)$, and $\|\eta(\theta)\mathrm{e}_2^H(\theta)\|^2$ are O $[(M-p+1)(M+p)]$ flops, $O((M-p+1)p)$ flops, and O $((M-p+1)M+1)$ flops, respectively. Consequently, the spectral search of the SRTRD-p-NC-MUSIC costs O $[J(-2p^2+2p+2M^2+2M+1)]$ flops.

Above all, we can obtain the number of total flops of the 2D-NC-MUSIC and the SRTRD-p-NC-MUSIC with the following form:

$$\begin{cases} C_{\text{2D}-\mathbf{NC}-\mathbf{MUSIC}} = \mathrm{O}\left(4M^2K\right) + \mathrm{O}\left(J^2(2M+1)(2M-K)\right), \\ C_{\mathbf{SRTRD}-\mathrm{p}-\mathbf{NC}-\mathbf{MUSIC}}(p) = \mathrm{O}\left(4M^2K\right) + \mathrm{O}\left((M-p)(M+p)(2M-K)\right) + \mathrm{O}\left(2M(2M-K)\right) + \mathrm{O}\left(J\left(-2p^2+2p+2M^2+2M+1\right)\right). \end{cases} \tag{25}$$

As it usually satisfies $J >> M > K$ in practice, the label (25) can be further approximated as follows:

$$\begin{cases} C_{\text{2D}-\mathbf{NC}-\mathbf{MUSIC}} \approx \mathrm{O}\left(J^2(2M+1)(2M-K)\right), \\ C_{\mathbf{SRTRD}-\mathrm{p}-\mathbf{NC}-\mathbf{MUSIC}}(p) \approx \mathrm{O}\left(J\left(-2p^2+2p+2M^2+2M+1\right)\right). \end{cases} \tag{26}$$

Obviously, the selection of the value of p depends on the following optimization problem:

$$\min_{p} C_{\mathbf{SRTRD}-p-\mathbf{NC}-\mathbf{MUSIC}}(p), \text{s.t.} 1 \le p \le M-K, \tag{27}$$

As shown in Figure 2, the label (26) is a quadratic function of p which is monotone decreasing if $p > 0.5$. Considering that p satisfies $1 \le p \le \mathrm{M}-\mathrm{K}$, we can get $C_{\mathbf{SRTRD}-\mathrm{p}-\mathbf{NC}-\mathbf{MUSIC}}(M-K) \le C_{\mathbf{SRTRD}-p-\mathbf{NC}-\mathbf{MUSIC}}(1)$ since the number of sensors and the number of sources usually satisfy $M > K$. Therefore, we can further get the optimal choice of p, which is represented as

$$p_{\text{opt}} = M - K. \tag{28}$$

3.5. Analysis of Computational Complexity. When $p = p_{\text{opt}}$, we substitute label (28) into label (26) and the computational complexity of the proposed SRTRD-p-NC-MUSIC can be further written, as shown in the following:

$$C_{\mathbf{SRTRD}-\mathrm{p}-\mathbf{NC}-\mathbf{MUSIC}}(p) = \mathrm{O}\left(J\left(4\mathrm{MK} + 4M + 1 - 2K^2 - 2K\right)\right). \tag{29}$$

Figure 3 illustrates the computational complexity comparison among the proposed SRTRD-p-NC-MUSIC, 2D-NC-MUSIC [21], RD-NC-MUSIC [23], and SRTRD-NC-MUSIC [26] with different numbers of sensors and different numbers of sources, where $J = 1000$ is considered. The RD-NC-MUSIC and the SRTRD-NC-MUSIC require $\mathrm{O}[J((2M-K)(4M+2)+M+2)]$ flops [23] and $\mathrm{O}(J(2M^2+2M+1))$ flops [26], respectively.

From Figure 3, we can see that the computational complexities of different algorithms increase with the number of sensors. Compared with the 2D-NC-MUSIC, the proposed SRTRD-p-NC-MUSIC can reduce the computational cost dramatically. Especially, the efficiency advantage of the proposed SRTRD-p-NC-MUSIC is more obvious in scenarios where the large numbers of sensors are applied. Moreover, the proposed SRTRD-p-NC-MUSIC can reduce the computational complexity to about 20% as compared to the RD-NC-MUSIC. Compared with the SRTRD-NC-MUSIC, the proposed SRTRD-p-NC-MUSIC can enhance the computational efficiency significantly when the large numbers of sensors are applied. In addition, unlike the 2D-NC-MUSIC and the RD-NC-MUSIC, the computational complexity of the proposed SRTRD-NC-MUSIC increases as the number of sources increases.

3.6. Summary of the Proposed Algorithm. The main steps of the proposed SRTRD-p-NC-MUSIC are shown as follows:

Step 1. Estimate the extended covariance matrix R_Y according to label (6).

Step 2. Perform the eigenvalue decomposition of the matrix $\boldsymbol{R}_Y$ according to label (5) to acquire the noise subspace $\mathbf{V}_N$.

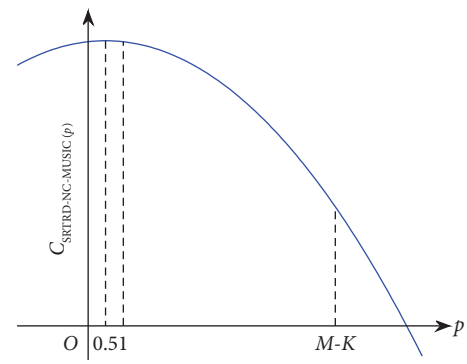

Figure 2: Analysis of the value of $C_{\text{SRTRD}-\mathrm{p}-\mathrm{NC}-\mathrm{MUSIC}}(p)$.

Step 3. Obtain the optimal choice of P according to label (28). Divide the matrix V_N according to label (9) to obtain $V_{N,2}$.

Step 4. Construct the new noise subspace V_{new} according to label (19). Divide the matrix $\tilde{\mathbf{A}}^H(\theta)$ according to label (20).

Step 5. Construct the one-dimensional spectral search function $P_{\mathbf{SRTRD}-p-\mathbf{NC}-\mathbf{MUSIC}}(\theta)$ according to label (24). Estimate the DoAs of the noncircular signals by searching K minimum values of label (24).

4. Simulation Results

In this section, we will demonstrate the effectiveness of the proposed SRTRD-p-NC-MUSIC, compared with the 2D-NC-MUSIC, RD-NC-MUSIC, and SRTRD-NC-MUSIC. For all simulations, a ULA with spacing $d = 0.5\lambda$ is used. In all experiments except for Figure 4, we set the number of sensors $M = 8$. We assume that the sources are narrow-band BPSK signals with equal power in the presence of the additive white Gaussian noise. All the simulation results are averaged via 3000 Monte Carlo runs. The Root Mean Square Error (RMSE) is defined as

$$\mathbf{RMSE} = \sqrt{\frac{1}{\mathrm{KN}_m}\sum_{k=1}^{K}\sum_{i=1}^{N_m}\left(\theta_{k,i} - \widehat{\theta}_{k,i}\right)^2}, \tag{30}$$

where N_m is the total number of the Monte Carlo simulations, and $\theta_{k,i}$, $\widehat{\theta}_{k,i}$ are the real value and estimated result of the kth source in the ith simulation, respectively. For the signals incoming from two similar directions, it is considered as the successful estimation when satisfying

$$\frac{P(\theta_1) + P(\theta_2)}{2} > P\left(\frac{\theta_1 + \theta_2}{2}\right), \tag{31}$$

where $P(\cdot)$ is the spectrum function, and θ_1, θ_2 are the incoming directions of the signals, respectively [29].

Figure 5 shows the DoA estimation results of the proposed SRTRD-p-NC-MUSIC and the 2D-NC-MUSIC, where $K = 3$ with $\theta = \{-45^\circ, -15^\circ, 5^\circ\}$ and the snapshots

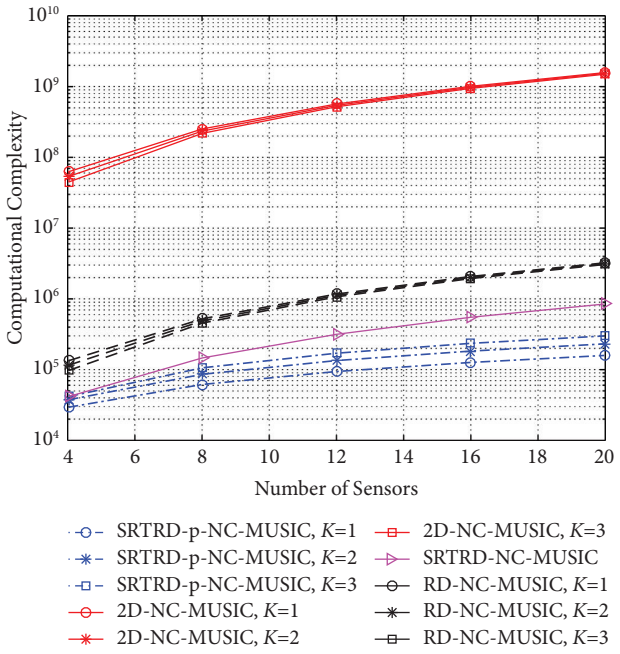

Figure 3: Comparison of computational complexities with a different number of sensors and a different number of sources.

$L = 1000$. The signal-to-noise ratio (SNR) is set to 5 dB. From Figure 5, the proposed SRTRD-p-NC-MUSIC can resolve all sources sufficiently well. Compared with the 2D-NC-MUSIC, the spatial spectrum of the SRTRD-p-NC-MUSIC has a sharper peak. In addition, the SRTRD-p-NC-MUSIC performs close to the 2D-NC-MUSIC and improves the computational efficiency significantly.

Figures 4, 6, and 7 indicate the RMSE performance comparison among the proposed SRTRD-p-NC-MUSIC, 2D-NC-MUSIC, RD-NC-MUSIC, and SRTRD-NC-MUSIC, where $K = 2$ sources with $\theta = \{-15^\circ, 20^\circ\}$. In Figure 6, the number of snapshots is fixed at 500, and the SNR is varied from −10 dB to 20 dB. It is clearly shown that the RMSEs of all algorithms in Figure 6 decrease as the SNR increases. Furthermore, the SRTRD-p-NC-MUSIC shows close RMSEs to the 2D-NC-MUSIC, and it has the better RMSE performance than the other three algorithms. In Figure 7, the SNR is fixed at 10 dB, and the number of snapshots is varied. From Figure 7, when the number of snapshots increases, the extended covariance matrix can be estimated more accurately, and the RMSEs of all algorithms in Figure 7 decrease. At the same time, the SRTRD-p-NC-MUSIC can achieve a better RMSE performance, close to that of the 2D-NC-MUSIC, than the other three algorithms. In Figure 4, the number of sensors is varied from 5 to 15, where SNR = 10 dB and $L = 500$. It is indicated that the RMSE performance of all algorithms in Figure 4 becomes better with increasing the number of sensors because the increasing number of sensors expands the aperture of the ULA. In addition, the SRTRD-p-NC-MUSIC still has a closer RMSE performance to the 2D-NC-MUSIC in comparison with the other three algorithms. Obviously, it can be seen clearly that the computational efficiency of the SRTRD-p-NC-MUSIC is improved without sacrificing too much estimation accuracy.

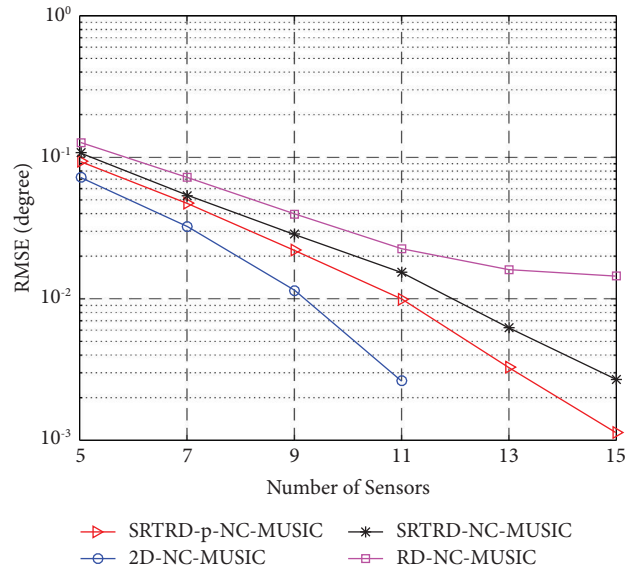

Figure 4: Performance comparison with a different number of sensors, SNR = 10 dB and $L = 500$.

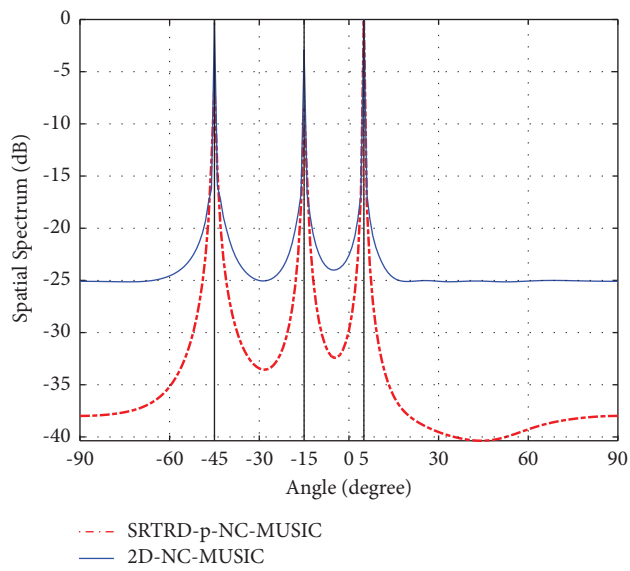

Figure 5: Spatial spectrum of the proposed SRTRD-p-NC-MUSIC and the 2D-NC-MUSIC, SNR = 5 dB and $L = 1000$.

In Sections 3.4 and 3.5, we have analysed how the choice of the value of p affects the computational complexity of the proposed SRTRD-p-NC-MUSIC. In order to investigate the estimation accuracy of the proposed SRTRD-p-NC-MUSIC, in Figure 8, we further compare the RMSE performance of the proposed algorithm with different choices of the value of p, where $K = 2$ sources with $\theta = \{-15^\circ, 20^\circ\}$. In Figure 8(a), we set the number of snapshots to be 500 and the SNRs from −10 dB to 20 dB. It can be seen that as the SNR increases, the RMSEs of all choices of the value of p decrease. In Figure 8(b), we set the SNR to be 10 dB, and the number of snapshots is varied. It is observed that the RMSEs of all choices of the value of p decrease with increasing the number of snapshots. In addition, from Figure 8(a) and Figure 8(b),

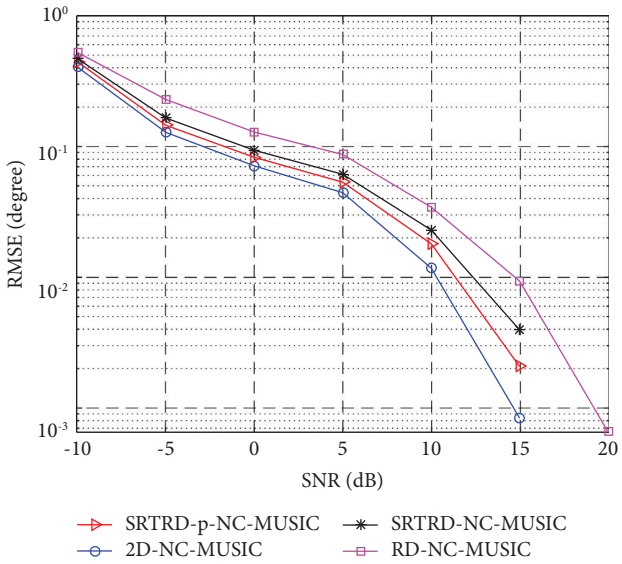

Figure 6: Performance comparison with different SNRs, $L = 500$.

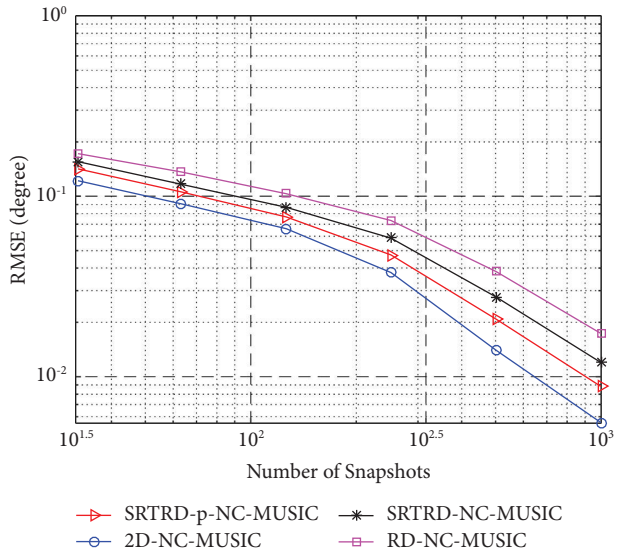

Figure 7: Performance comparison with a different number of snapshots, SNR = 10 dB.

we can see that when the choice of the value of p is closer to the optimum p_{opt}, the RMSE performance of the proposed algorithm is much better. This is because as the value of p is closer to the optimum p_{opt}, the orthogonality between the reconstructed noise subspace and the space spanned by the columns of the extended manifold matrix is more improved [29, 35].

In Figures 9 and 10, there are two signals impinging upon the ULA from the directions $\theta_1 = 10^\circ$ and $\theta_2 = 11^\circ$. Here, the number of the snapshots is 500. Figure 9 illustrates the DoA resolution performance versus different SNRs, where two sources are located at similar directions. It is can be observed that these four algorithms in Figure 9 have a 100% resolution probability to distinguish the two sources when the SNR is higher than 5 dB. However, the SRTRD-p-NC-MUSIC can obtain much better spatial resolution than the other three algorithms when the SNR is lower than 0 dB. This is because the reconstruction of the noise subspace improves the orthogonality between the signal subspace and the noise subspace and the dimension of the reconstructed noise subspace is reduced significantly, which leads to a sharper peak of the spatial spectrum [29, 35]. In Figure 10, the DoA estimation results of the proposed SRTRD-p-NC-MUSIC and the 2D-NC-MUSIC are depicted for 10 simulations, where SNR = 5 dB. We can see that the spectral peak of the SRTRD-p-NC-MUSIC is sharper than that of the 2D-NC-MUSIC, and the SRTRD-p-NC-MUSIC achieves a better performance than the 2D-NC-MUSIC when distinguishing two signals from similar directions. The simulation results in Figure 10 also verify the experimental results in Figure 9.

Figure 11 depicts the resolution probability comparison versus different intersource spacing $\Delta\theta$ among the proposed SRTRD-p-NC-MUSIC, 2D-NC-MUSIC, RD-NC-MUSIC, and SRTRD-NC-MUSIC, where SNR = 0 dB and the snapshots $L = 500$. It is considered that two sources are located at 20° and $(20+\Delta\theta)^\circ$, where $\Delta\theta$ represents the intersource spacing. We can see that when the intersource spacing $\Delta\theta$ is not less than 1.8°, these four algorithms have a 100% resolution probability to identify the two sources. Especially, the proposed SRTRD-p-NC-MUSIC can distinguish the two sources accurately when the intersource spacing $\Delta\theta$ is greater than 1°. Compared with the other three algorithms, the SRTRD-p-NC-MUSIC can achieve much better spatial resolution when the intersource spacing is less than 1° due to the better orthogonality between the signal subspace and the noise subspace and the sharper peak of the spatial spectrum [29, 35], which is also verified by the simulation results in Figure 10.

Figure 12 indicates the running time comparison among the proposed SRTRD-p-NC-MUSIC, 2D-NC-MUSIC, RD-NC-MUSIC, and SRTRD-NC-MUSIC versus different number of sensors. The simulation parameters are set as SNR = 10 dB, $L = 500$, $K = 2$ and $\theta = \{-10^\circ, 25^\circ\}$. The searching interval is fixed at 0.05°. The running times in Figure 12 are given by running the MATLAB codes on a PC with an Intel (*R*) Core (TM) i5-5300U processor, a 2.3 GHz CPU, and 2 GB RAM in the same environment. It can be observed that the SRTRD-p-NC-MUSIC costs much lower running time than the other three algorithms. Specifically, as the number of sensors increases, the running times of all algorithms in Figure 12 increase. Simultaneously, the efficiency advantage of the SRTRD-p-NC-MUSIC is more obvious with increasing the number of sensors, which are consistent with the aforementioned computational complexity analysis. In Figure 12(a), compared with the 2D-NC-MUSIC, the SRTRD-p-NC-MUSIC only needs a one-dimensional peak searching, and furthermore, the reconstruction of the noise space efficiently avoids the redundancy computations in the one-dimensional peak searching due to the rank deficiency of the noise subspace. Therefore, the SRTRD-p-NC-MUSIC can reduce the computational complexity to less than 3% as compared to the 2D-NC-MUSIC. In Figure 12(b), the dimension of the

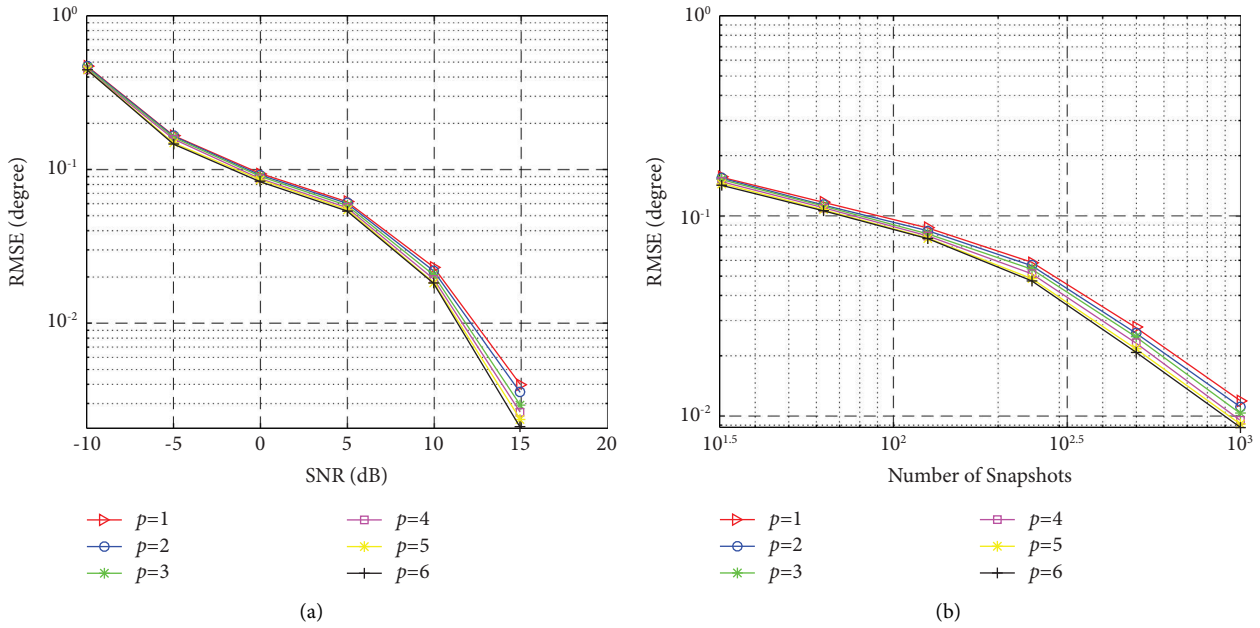

Figure 8: Performance comparison of the proposed SRTRD-p-NC-MUSIC with different choices of the value of p. (a) RMSEs with different SNRs, $L = 500$. (b) RMSEs with a different number of snapshots, SNR = 10 dB.

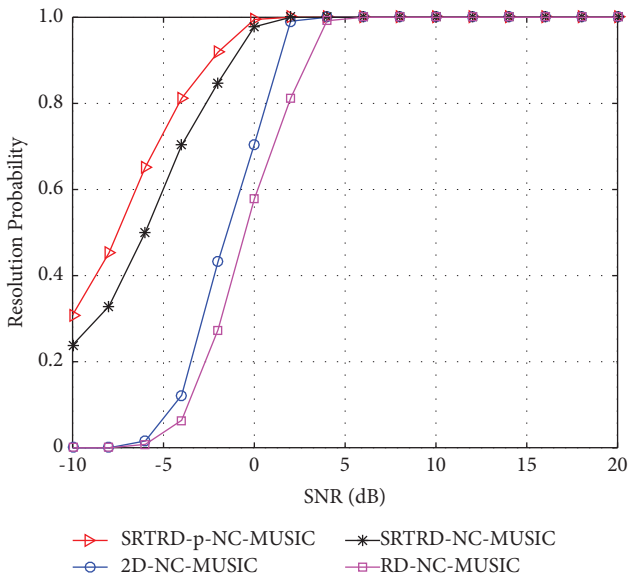

Figure 9: Resolution probability comparison with different SNRs, $L = 500$.

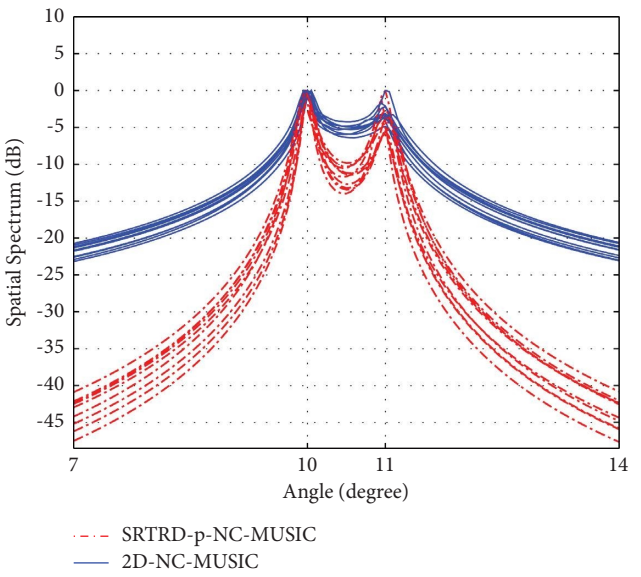

Figure 10: Spatial spectrum of the proposed SRTRD-p-NC-MUSIC and the 2D-NC-MUSIC for 10 simulations, SNR = 5 dB and $L = 500$.

reconstructed noise space of the SRTRD-p-NC-MUSIC is descended and the redundancy computations of the one-dimensional peak searching of the SRTRD-p-NC-MUSIC are removed, and so, the computational complexity of the SRTRD-p-NC-MUSIC is reduced to less than 20% as compared to the RD-NC-MUSIC. In Figure 12(c), compared with the SRTRD-NC-MUSIC, the SRTRD-p-NC-MUSIC can more completely remove the redundancy computations in the one-dimensional peak searching according to a novel block matrix method. Consequently, from Figure 12(c), we can see that the computational complexity of the SRTRD-p-NC-MUSIC is lower than that of the SRTRD-NC-MUSIC.

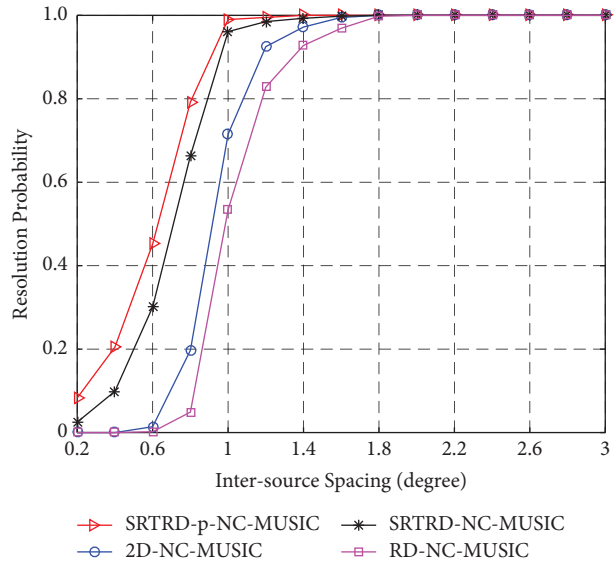

Figure 11: Resolution probability comparison versus different intersource spacing $\Delta\theta$, SNR = 0 dB and $L = 500$.

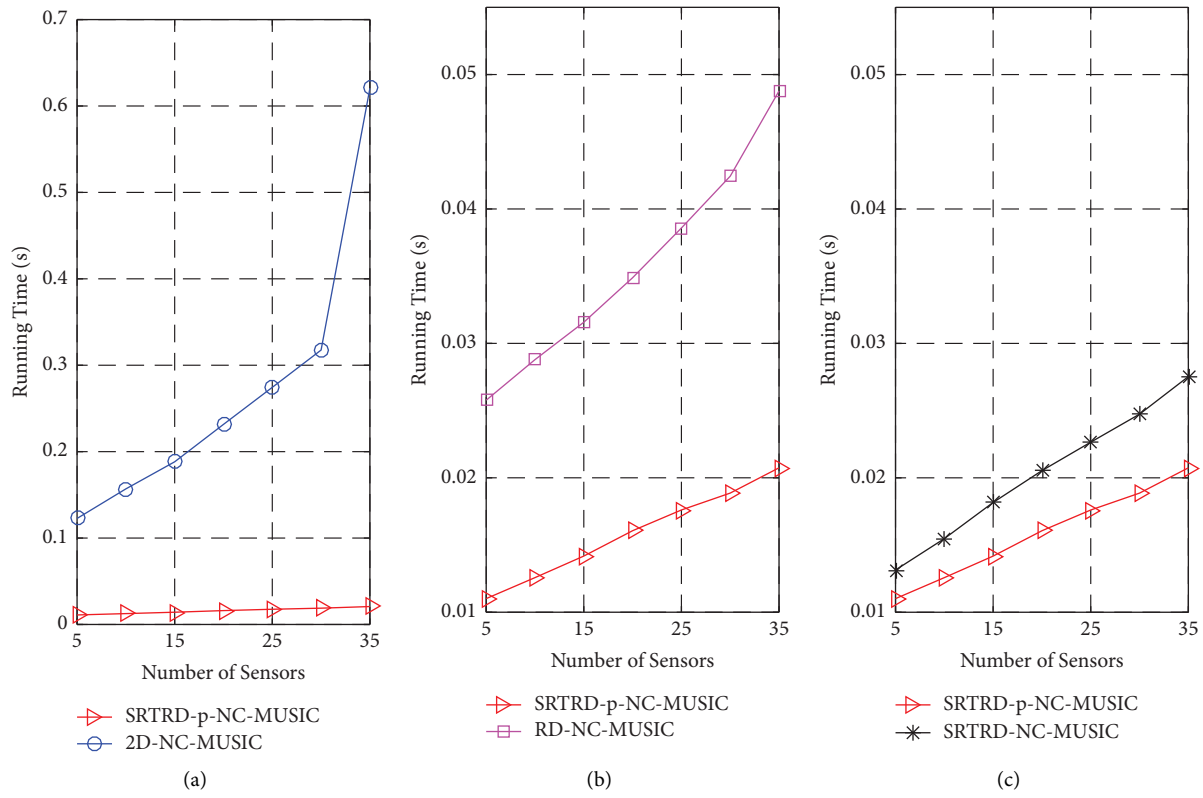

Figure 12: Running time comparison with a different number of sensors, SNR = 10 dB and $L = 500$.

5. Conclusions

In this paper, we have proposed the SRTRD-p-NC-MUSIC algorithm for the DoA estimation of NC signals in order to reduce the computational complexity of the conventional 2D-NC-MUSIC algorithm. The proposed SRTRD-p-NC-MUSIC algorithm not only converts the two-dimensional peak searching into the one-dimensional peak searching, but also utilizes the block matrix method and SRT to efficiently avoid the redundancy computations in the one-dimensional peak searching due to the rank deficiency of the noise subspace. Compared with the 2D-NC-MUSIC algorithm, the proposed SRTRD-p-NC-MUSIC algorithm can dramatically improve the computational efficiency on the premise of ensuring the accuracy of DOA estimation, especially in scenarios where large numbers of sensors are applied.

Data Availability

The data used to support the findings of this study are available from the corresponding author upon request.

Conflicts of Interest

The authors declare that they have no conflicts of interest.

Acknowledgments

This research was funded by the Natural Science Special Foundation of Shaanxi Provincial Department of Education (Grant no.20JK0966), the Natural Science Foundation of Shaanxi Province (Grant no. 2023-JC-QN-0756), and the National Natural Science Foundation of China (Grant nos. 62172338 and 62072378).

References

[1] L. Wan, K. Liu, Y. C. Liang, and T. Zhu, "DOA and polarization estimation for non-circular signals in 3-D millimeter wave polarized massive MIMO systems," *IEEE Transactions on Wireless Communications*, vol. 20, no. 5, pp. 3152–3167, 2021.

[2] Y. Wang, W. Wu, X. Zhang, and W. Zheng, "Transformed nested array designed for DOA estimation of non-circular signals: reduced sum-difference co-array redundancy perspective," *IEEE Communications Letters*, vol. 24, no. 6, pp. 1262–1265, 2020.

[3] X. Dong, X. Zhang, J. Zhao, and M. Sun, "Non-circular sources DOA estimation for coprime array with impulsive noise: a novel augmented phased fractional low-order moment," *IEEE Transactions on Vehicular Technology*, vol. 71, no. 10, pp. 10559–10569, 2022.

[4] B. Yao, Z. Dong, W. Zhang, W. Wang, and Q. Wu, "Degree-of-freedom strengthened cascade array for DOD-DOA estimation in MIMO array systems," *Sensors*, vol. 18, no. 5, pp. 1557–1577, 2018.

[5] F. Mei, H. Xu, W. Cui, B. Ba, and Y. Wang, "A transformed coprime array with reduced mutual coupling for DOA estimation of non-circular signals," *IEEE Access*, vol. 9, no. 5673, pp. 125984–125998, 2021.

[6] Z. Lin, T. Lv, W. Ni, J. A. Zhang, and R. P. Liu, "Nested hybrid cylindrical array design and DOA estimation for massive IoT networks," *IEEE Journal on Selected Areas in Communications*, vol. 39, no. 4, pp. 919–933, 2021.

[7] Q. Tian, T. Qiu, J. Ma, J. Li, and R. Li, "Robust fractional lower order correntropy algorithm for DOA estimation in impulsive noise environments," *IEICE - Transactions on Communications*, vol. 104, no. 1, pp. 35–48, 2021.

[8] P. Gupta and M. Agrawal, "Design and analysis of the sparse array for DOA estimation of noncircular signals," *IEEE Transactions on Signal Processing*, vol. 67, no. 2, pp. 460–473, 2019.

[9] F. G. Yan, J. Wang, S. Liu, B. Cao, and M. Jin, "Computationally efficient direction of arrival estimation with unknown number of signals," *Digital Signal Processing*, vol. 78, no. 3154, pp. 175–184, 2018.

[10] R. Schmidt, "Multiple emitter location and signal parameter Estimation," *IEEE Transactions on Antennas and Propagation*, vol. 34, no. 3, pp. 276–280, 1986.

[11] M. Rubsamen and A. Gershman, "Direction-of-Arrival estimation for nonuniform sensor arrays: from manifold separation to fourier domain MUSIC methods," *IEEE Transactions on Signal Processing*, vol. 57, no. 2, pp. 588–599, 2009.

[12] R. Roy and T. Kailath, "ESPRIT-estimation of signal parameters via rotational invariance techniques," *IEEE Transactions on Acoustics, Speech, & Signal Processing*, vol. 37, no. 7, pp. 984–995, 1989.

[13] J. J. Cai, W. Liu, R. Zong, and Y. Dong, "A MUSIC-Type DOA estimation method based on sparse arrays for a mixture of circular and non-circular signals," in *Proceedings of the 2020 IEEE International Conference on Signal Processing, Communications and Computing(ICSPCC)*, pp. 21–24, Macau, China, August 2020.

[14] X. T. Meng, F. G. Yan, S. Liu, Y. Zhang, and M. Jin, "Real-valued DOA estimation for non-circular sources via reduced-order polynomial rooting," *IEEE Access*, vol. 7, pp. 158892–158903, 2019.

[15] L. P. Teng, Q. Wang, H. Chen, W. P. Zhu, W. Liu, and J. Cai, "DOA estimation for coexistence of circular and non-circular signals based on atomic norm minimization," in *Proceedings of the 2020 IEEE 11th Sensor Array and Multichannel Signal Processing Workshop (SAM)*, pp. 8–11, Hangzhou, China, June 2020.

[16] P. Han, H. W. Xu, B. Ba, and Y. Zhang, "Direction-of-arrival estimation in a mixture of multiple circular and non-circular signals using nested array," *IEEE Access*, vol. 8, no. 1454, pp. 105237–105249, 2020.

[17] Y. Wang, J. Shen, X. Zhang, H. Yi, and D. Xiangrui, "Non-circular signals for nested array: sum-difference co-array and DOA estimation algorithm," *IET Radar, Sonar and Navigation*, vol. 14, no. 1774, pp. 27–35, 2020.

[18] W. Zheng, X. Zhang, Y. Wang, M. Zhou, and Q. Wu, "Extended coprime array configuration generating large-scale antenna Co-array in massive MIMO system," *IEEE Transactions on Vehicular Technology*, vol. 68, no. 8, pp. 7841–7853, 2019.

[19] C. Zhou, Y. Gu, X. Fan, Z. Shi, G. Mao, and Y. D. Zhang, "Direction-of-arrival estimation for coprime array via virtual array interpolation," *IEEE Transactions on Signal Processing*, vol. 66, no. 22, pp. 5956–5971, 2018.

[20] Z. Chen, Y. Ding, S. Ren, and Z. Chen, "A novel noncircular MUSIC algorithm based on the concept of the difference and sum coarray," *Sensors*, vol. 18, no. 2, pp. 344–360, 2018.

[21] C. Adnet, P. Gounon, and J. Galy, "High resolution array processing for non circular signals," in *Proceedings of the 9th European Signal Processing Conference (EUSIPCO 1998)*, Rhodes, Greece, September 1998.

[22] P. Charge, Y. Wang, and J. Saillard, "A non-circular sources direction finding method using polynomial rooting," *Signal Processing*, vol. 81, no. 8, pp. 1765–1770, 2001.

[23] H. Sun, W. Zheng, and W. Lv, "Reduced-dimension NC-MUSIC algorithm for DOA estimation of noncircular signals in linear array," *Aero Weaponry*, vol. 2016, Article ID 348636, 9 pages, 2016.

[24] L. He, X. P. Lin, C. Ge, M. J. Zhou, and X. F. Zhang, "Noncircular signal DOA estimation with reduced dimension MUSIC for coprime linear array," in *Proceedings of the 2018 4th Annual International Conference on Network and Information Systems for Computers (ICNISC)*, pp. 19–21, Wuhan, China, April 2018.

[25] W. H. Lv, H. P. Sun, X. Zhang, and D. Xu, "Reduced-dimensionnoncircular-capon algorithm for DOA estimation

of noncircular signals," *International Journal of Antennas and Propagation*, vol. 2015, Article ID 348636, 9 pages, 2015.

[26] W. Wang, M. Zhang, and B. B. Yao, "Computationally efficient direction-of-arrival estimation of non-circular signal based on subspace rotation technique," *Journal on Communications*, vol. 41, no. 295, pp. 198–205, 2020.

[27] W. J. Tan, X. A. Feng, and X. P. Zhang, "DOA estimation of non-circular signals based on Euler transformation sparse reconstruction," *Journal of Detection and Control*, vol. 40, no. 3057, pp. 63–67, 2018.

[28] Z. M. Liu, Z. T. Huang, Y. Y. Zhou, and J. Liu, "Direction-of-arrival estimation of noncircular signals via sparse representation," *IEEE Transactions on Aerospace and Electronic Systems*, vol. 48, no. 3, pp. 2690–2698, 2012.

[29] F. G. Yan, X. H. Qi, and S. Liu, "Low-complexity DOA estimation via subspace rotation technique," *Journal of Electronics and Information Technology*, vol. 38, no. 2157, pp. 629–634, 2016.

[30] C. H. Zheng, H. H. Deng, and G. Yang, "MUSIC algorithm about real values for noncircular signals based on instrumental sensors," *Systems Engineering and Electronics*, vol. 38, no. 33546, pp. 2469–2473, 2016.

[31] H. Abeida and J. P. Delmas, "MUSIC-like estimation of direction of arrival for noncircular sources," *IEEE Transactions on Signal Processing*, vol. 54, no. 7, pp. 2678–2690, 2006.

[32] L. T. Wan and L. H. Xie, "An improved DOA estimation algorithm for circular and non-circular signals with high resolution," in *Proceedings of the 2016 IEEE International Conference on Acoustics, Speech and Signal Processing (ICASSP)*, Shanghai, China, March 2016.

[33] G. H. Golub and C. F. Van Loan, *Matrix Computations*, The Johns Hopkins University Press, Baltimore, MD, USA, 1996.

[34] G. Xu and T. Kailath, "Fast subspace decomposition," *IEEE Transactions on Signal Processing*, vol. 42, no. 21317, pp. 539–551, 1999.

[35] F. G. Yan, S. Liu, M. Jin, and X. L. Qiao, "2-D DOA estimation method based on dimension descended noise subspace," *Journal of Electronics and Information Technology*, vol. 34, pp. 832–837, 2012.